GEOFLUIDS

Geofluids (2011) **11**, 71–86 doi: 10.1111/j.1468-8123.2010.00312.x

Origin of palaeo-waters in the Ordovician carbonates in Tahe oilfield, Tarim Basin: constraints from fluid inclusions and Sr, C and O isotopes

K. LI[1,2], C. CAI[1], H. HE[3], L. JIANG[1,2], L. CAI[1,2], L. XIANG[1,2], S. HUANG[4] AND C. ZHANG[5]

[1]Key Lab of Petroleum Resources, Institute of Geology and Geophysics, Chinese Academy of Sciences, Beijing, China; [2]Graduate University of Chinese Academy of Sciences, Beijing, China; [3]Institute of Petroleum Exploration and Development, CENOPEC, Beijing, China; [4]State Key Lab Oil Gas Reservoir Geology and Exploitation, Institute of Sedimentary Geology, Chengdu University of Technology, Chengdu, China; [5]Department of Geochemistry, Yangtze University, Jingzhou, Hubei, China

ABSTRACT

Petrographic features, isotopes, and trace elements were determined, and fluid inclusions were analyzed on fracture-filling, karst-filling and interparticle calcite cement from the Ordovician carbonates in Tahe oilfield, Tarim basin, NW China. The aim was to assess the origin and evolution of palaeo-waters in the carbonates. The initial water was seawater diluted by meteoric water, as indicated by bright cathodoluminescence (CL) in low-temperature calcite. The palaeoseawater was further buried to temperatures from 57 to 110°C, nonluminescent calcite precipitated during the Silurian to middle Devonian. Infiltration of meteoric water of late Devonian age into the carbonate rocks was recorded in the first generation of fracture- and karst-filling dull red CL calcite with temperatures from <50°C to 83°C, low salinities (<9.0 wt%), high Mn contents and high $^{86}Sr/^{87}Sr$ ratios from 0.7090 to 0.7099. During the early Permian, ^{87}Sr-rich hydrothermal water may have entered the carbonate rocks, from which precipitated a second generation of fracture-filling and interparticle calcite and barite cements with salinities greater than 22.4 wt%, and temperatures from 120°C to 180°C. The hydrothermal water may have collected isotopically light CO_2 (possibly of TSR-origin) during upward migration, resulting in hydrothermal calcite and the present-day oilfield water having $\delta^{13}C$ values from −4.3 to −13.8‰ and showing negative relationships of $^{87}Sr/^{86}Sr$ ratios to $\delta^{13}C$ and $\delta^{18}O$ values. However, higher temperatures (up to 187°C) and much lower salinities (down to 0.5 wt%) measured from some karst-filling, giant, nonluminescent calcite crystals may suggest that hydrothermal water was deeply recycled, reduced (Fe-bearing) meteoric water heated in deeper strata, or water generated from TSR during hydrothermal water activity. Mixing of hydrothermal and local basinal water (or diagenetically altered connate water) with meteoric waters of late Permian age and/or later may have resulted in large variations in salinity of the present oilfield waters with the lowest salinity formation waters in the palaeo-highs.

Key words: carbon isotopes, carbonates, fluid inclusion, fracture-filling, hydrothermal water, strontium isotopes, Tarim basin

Received 25 November 2009; accepted 16 August 2010

Corresponding author: Prof. Dr. Chunfang Cai, Key Lab of Petroleum Resources, Institute of Geology and Geophysics, Chinese Academy of Sciences, Beitucheng Xilu 19, Beijing 100029, China.
Email: cai_cf@mail.iggcas.ac.cn. Tel: 86-10-82998127. Fax: 86-10-62010846.

Geofluids (2011) **11**, 71–86

INTRODUCTION

The Tahe oilfield is located in the Tabei Uplift, north of the Tarim Basin, NW China, with giant volumes of petroleum reservoired in Ordovician carbonates with small volumes of condensate in the Cambrian dolomites at a depth of 8402 m in well TS1(Fig. 1). Abundant pores, factures and vugs exist in the reservoirs even at 8400 m. Previous studies showed that the porosity in this area resulted from meteoric dissolution of carbonates during Caledonian and early Hercynian Orogenies (Yan 2002; Yu 2005; Qian *et al.* 2007; Zhang *et al.* 2007), when the strata were

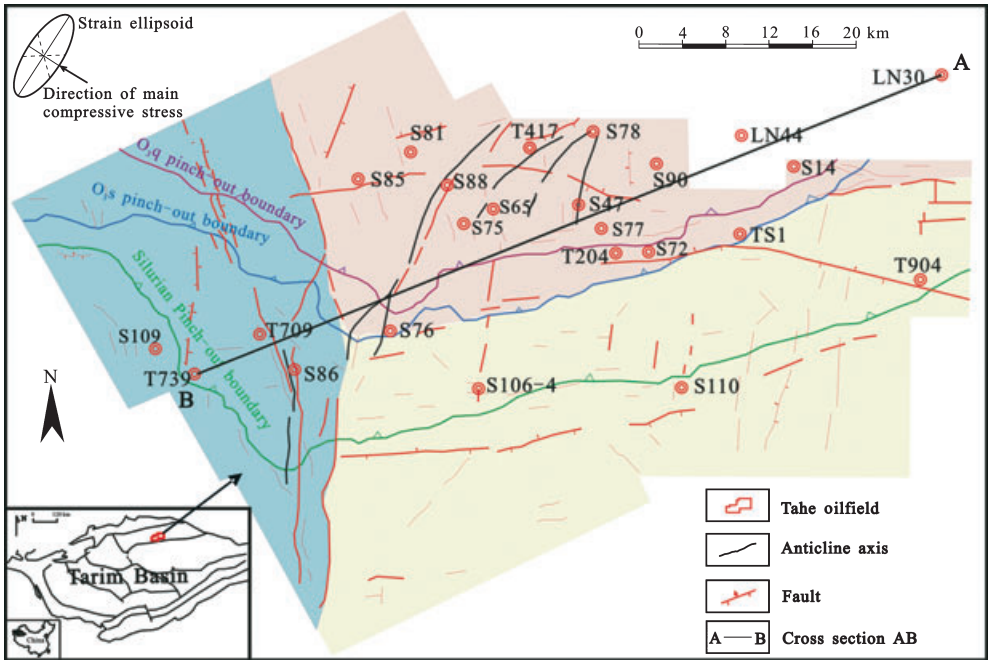

Fig. 1. Map showing the geology, tectonics and locations of sampled wells.

uplifted and exposed to the surface. However, this mechanism alone cannot account for high porosity in the reservoirs away from the unconformities, where meteoric water supply would have been limited, or in the deep reservoirs (e.g. >6000 m), where most pore space is typically completely destroyed because of compaction and cementation (Halley & Schmoker 1983).

Carbonate dissolution by hydrothermal water has been invoked to explain ''sag'' occurrences above porous hydrothermal dolomite in deep carbonates in some petroleum-producing basins (Davies & Smith 2006). In the Central Tarim Basin, fracture-filling barite, fluorite, and pyrite probably originated from hydrothermal activity (Cai *et al.* 2008). However, it is not clear whether there has been hydrothermal activity in the Tahe oilfield, because the chemical and isotopic composition of Sr, C, and O and thus the source of hydrothermal water have not previously been characterized. The specific question being addressed in this study is the origin and evolution of palaeo-waters in the carbonates in the northern Tarim Basin.

To address this issue, this paper presents fluid-inclusion data, trace element compositions, and strontium, carbon, and oxygen isotopes from the fracture-filling, karst-filling and interparticle calcite cements and formation water in the Ordovician in Tahe area. Fluid-inclusion data can be used to indicate temperatures and salinities during mineralization, and Sr, C, and O isotopic compositions have widely been used to indicate the origin of waters, mixing of different water bodies, and cross-formation water flow (Worden & Matray 1995; Cai *et al.* 2001a,b, 2008; Schwinn *et al.* 2006; Worden *et al.* 2006; Sandstrom & Tullborg 2009). Analysis of these types of data is expected to supply reliable information to address the source and evolution of the water in this field.

GEOLOGICAL SETTING

The Tarim basin, which is located in northwest of China (Fig. 1), has a long history of successful petroleum exploration. Recently, giant petroleum resources have been found in reef-shoal facies limestone in the Ordovician in the Central Tarim and Tabei uplifts (Fig. 1). Detailed descriptions of the geological settings of the Tarim Basin have been published previously (Cai *et al.* 2001a,b, 2008). In brief, Upper Proterozic (Sinian) beach to shallow marine facies siliciclastic rock and carbonates lie on Archean and Proterozoic crystalline basement. The overlying Cambrian and Ordovician strata are composed of platform facies limestone and dolomite, slope facies limestone and marlstone, and basinal facies mudstone, shale and marlstone. The Silurian to Carboniferous sequence consists of marine sandstone and mudstone. Permian strata are composed of lacustrine sediment and volcanic rock. Following the emergence of the sediments, Mesozoic and Cenozoic units are represented by nonmarine fluvial sandstone and mudstone.

Various orogenic events have led to nine recognized unconformities in the basin (Table 1).In the Tabei area, thrusting and uplift in the north of the Tahe area was significantly greater than in the south as a result of different structural stresses during the late Caledonian Orogeny at

the end of Ordovician. Thus, Middle-Upper Ordovician strata in the north were completely removed by erosion, whereas the strata remain in the south (Fig. 2). No Devonian or Silurian strata remain in the majority of the Tabei area as a result of the early Hercynian Orogeny at the end of the Devonian. Multiple-stage orogenies in the Tabei area also created abundant polyphase faults besides the unconformities. During the Sinian to late Cambrian stages, the study area was in a continental rift setting. Accordingly, a series of NW, NE, EW, and SN strike normal faults developed under the control of NE-SW, NNE-SSW, NNW-SSE trending primary stresses. Subsequently, as a result of middle-late Caledonian Orogeny, Cambro-Ordovician formations were in an extensional setting instead of the previous compressive environment. Extensive NW, NE, EW, and SN strike thrust faults developed. The orientation of the faults formed during the middle-late Caledonian Orogenny is consistent with that of the faults formed during the Sinian to late Cambrian. Therefore, a complex of deep-seated faults existed which affected the Cambro-Ordovician formations in the Tahe oilfield.

Burial and thermal history modeling of Wells S109 in the south and S75 in the north of the Tahe area, using Thermodel software (Hu & Zhang 1998) and calibriated with vitrinite reflectance (R_o) data, shows that rapid sedimentation took place during the late Ordovician to early Silurian, late Devonian to early Carboniferous, and late Permian to the Neogene. Significant uplift occurred during the late Silurian, the end of the Devonian to early Carboniferous, and the late Permian (Fig. 3). The Ordovician strata did not experience temperatures more than 110°C prior to the late Hercynian Orogeny during the late Permian and exceeded this temperature only after the Eocene. Present-day temperatures of Ordovician strata have temperatures up to 130°C in the north and up to 150°C in the south.

Table 1 Synthetic stratigraphy for Tahe area, Tabei Uplift.

Stratigraphic system					
Erathem	System	Series	Stage	Thickness (m)	Lithology
Cenozoic	Quaternary		Q	16–63	Grayish-yellow sand and clay
	Neogene	Pliocene	N_2k	1522–2009	Gray siltstone and brownish yellow mudstone
		Miocene	N_1k	732–1052	Gray siltstone and brown mudstone
			N_1j	329–674	Gray and grayish-green mudstone, siltstone and sandstone
			N_1s	38–326	Light yellow, brown fine-grained sandstone and siltstone
	Paleogene		K_2–E	614–745	Brownish-red sandstone, mudstone and siltstone
Mesozoic	Cretaceous	Upper			
		Lower	K_1kp	298–436	Tan silty-mudstone, mudstone and grayish-green sandstone
	Jurassic	Lower	J_1	42–76	Gray fine-grained sandstone, mudstone, silty stone with thin layer of coal
	Triassic	Upper	T_3h	98–174	Dark gray, gray mudstone, blacks and fine-grained sandstone
		Middle	T_2a	176–298	The upper part is dark gray and black mudstone, and the lower is sandstone
		Lower	T_1k	40–120	Gray, dark gray mudstone
Paleozoic	Carboniferous	Lower	C_1kl	370–537	Gray, tawny brown mudstone, light gray sandstone and marlstone
			C_1b	76–235	Gray micrite, motleysandstone, mudstone, and grainstone
	Ordovician	Upper	O_3s	0–500	Grayish green and gray mudstone and micritic limestone
			O_3l		The middle-upper part is grayish green silty-mudstone, silty-micrite and micrite, and the lower is deep grey bioclastic marlstone and micrite
			O_3q		Motley packstone and micrite
				>427	Gray-brownish gray calcarenite, bioclastic marlstone, oolitic limestone
		Middle	O_2yj		The upper part is gray micrite and calcarenite, and the lower is interbeded limestone and dolostone
			$O_{1\text{-}2}y$		
		Lower	O_1p		Grey dolomite, calcareous dolomite and dolomitic limestone
	Cambrian	Upper	ε_3q1	1524	Gray argillaceous dolomite and fine to coarse-crystalline dolomite

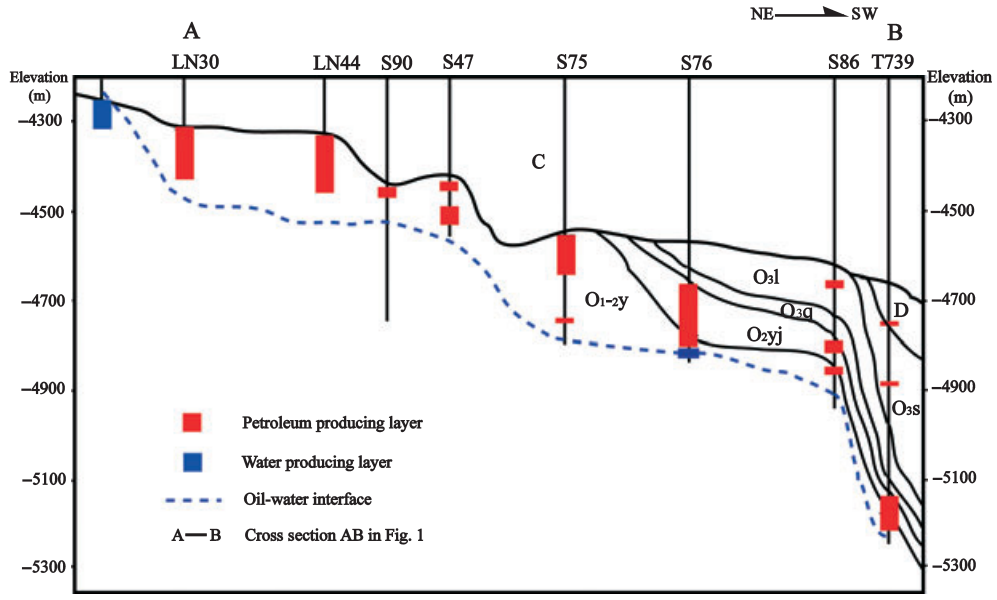

Fig. 2. Cross section AB of the Tahe oilfield shows different formation contacts in the south and the north and water-oil distribution.

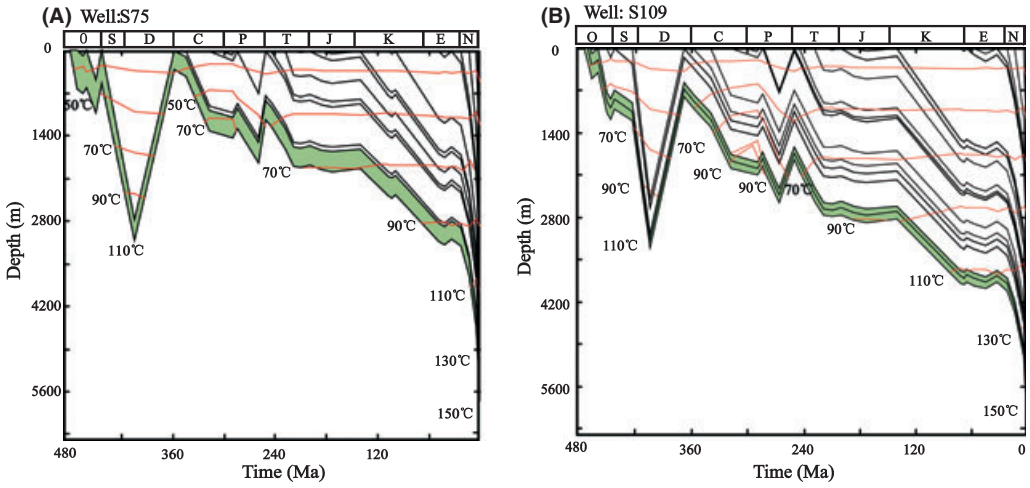

Fig. 3. Graph of burial-thermal history of wells S109 in the south (A) and S75 in the north (B).

SAMPLING AND ANALYTICAL METHODS

Thirty-nine core samples from seventeen wells across the whole Tahe oilfield (Fig. 1) were collected from the Ordovician strata. The samples with veins, giant calcite crystals, or different generations of cements were chosen from the petroleum reservoirs. Petrographic and cathodoluminescence (CL) analyses were performed on 23 thin sections. A cold cathode luminescence microscope was used with a beam voltage of 16.3 kV, a current of 325 μA and a beam diameter of 4 mm. Fluid inclusions were observed under a Linkam THMSG 600 fitted a UV lamp to determine whether they were oil or aqueous inclusions. Micro-thermometric measurements were conducted using the THMSG 600 freezing/heating stage with precision of ±1°C. Salinity was calculated based on the ice final melting temperature measurement using the following equation:

Salinity = $0.00 + 1.78T_m - 0.0442T_m^2 + 0.000557T_m^3$ (Bodnar 1993), where T_m is the depression of the freezing point in degrees Celsius (°C).

Fracture-fillings with a width of more than 2 mm were extracted from core using a dentist's drill and subject to trace element analyses and carbon, oxygen, and strontium isotope measurement. For carbon and oxygen isotope analyses, about 30–50 mg of samples was reacted overnight with 100% phosphoric acid at 25°C under vacuum to release CO_2 from calcite. The CO_2 was then analyzed for carbon and oxygen isotopes on a Finnigan MAT251 mass

spectrometer standardized with NBS-18. All carbon and oxygen data are reported in per mil relative to the Vienna Peedee Belemnite (VPDB) standard, respectively. The precision for $\delta^{13}C$ and $\delta^{18}O$ measurement is ±0.1‰. For strontium isotope analyses, 50–100 mg of sample powders was dissolved in 2.5 N HCl, and the strontium was then extracted using the conventional cation exchange procedures. The $^{87}Sr/^{86}Sr$ ratios were measured on a Finnigan MAT-261 mass spectrometer. The $^{87}Sr/^{86}Sr$ ratios were corrected relative to the NBS987 standard. The precision for $^{87}Sr/^{86}Sr$ measurement is ±0.00003–0.00007, respectively. Trace elements were analyzed using a Finnigan ICP-MS. Repeated analysis on standards and samples gives precisions better than ±8%. Mn was measured using an AA2610 atomic absorption spectrometer with a detection limit of 0.01% and precisions better than ±8%, and Fe was measured by colorimetry using RPA-100Fe equipment with a detection limit of 5 $\mu g\ g^{-1}$ and precisions better than ±13%.

RESULTS

Petrology of fracture-fillings and cements

Calcite and a small amount of barite were observed to occur as fracture-, karst-, and vug-fillings or as interparticle cement. There are three different types of fractures, which are as follows: type I occurs in irregular shapes and is distributed as networks (Fig. 4A), type II and type III have straight and elongated shapes with type II fracture-filling

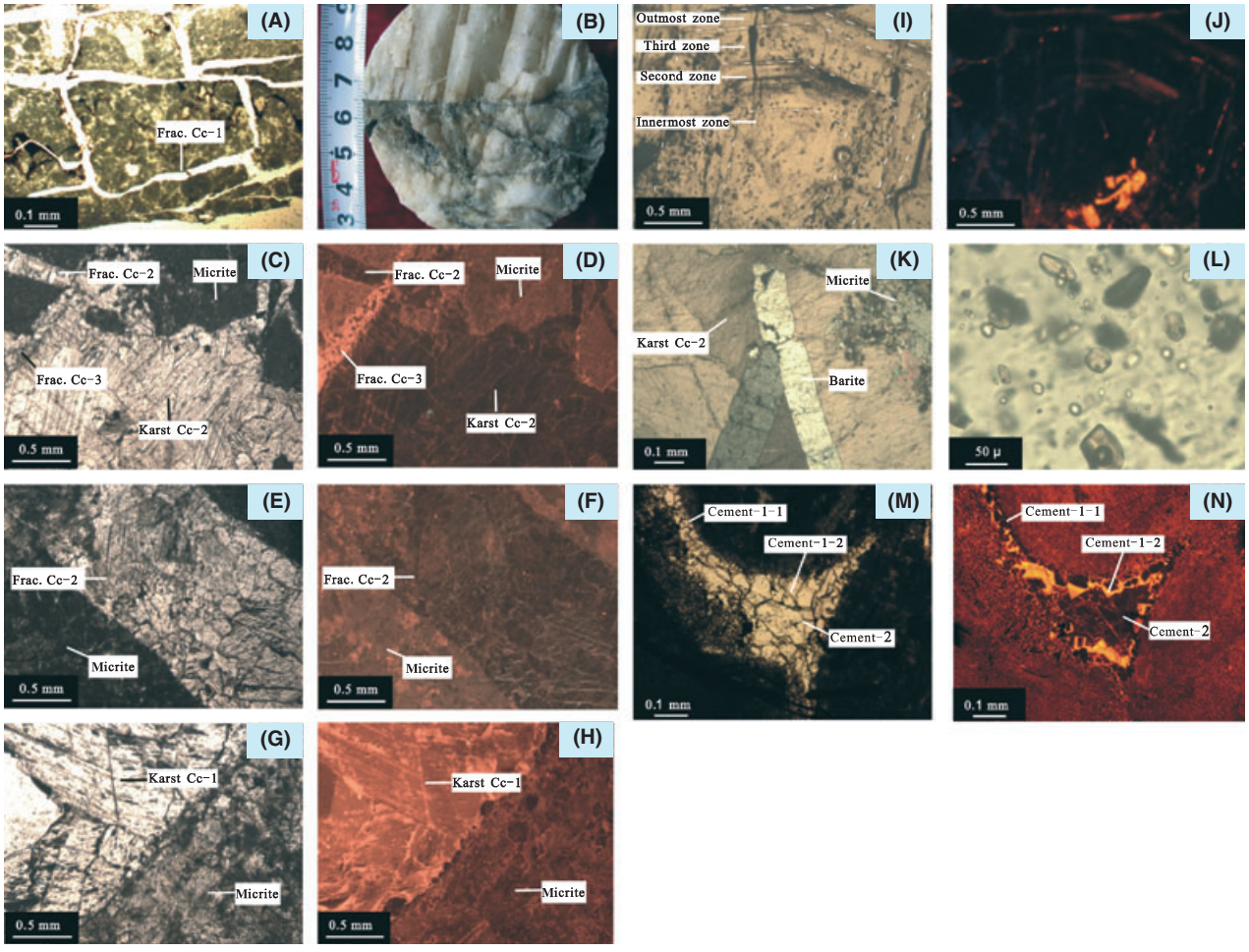

Fig. 4. Photographs showing different types of calcite and barite. (A) type I irregular fracture-fillings at 6088 m in Well S119, O_{2yj}, planar polarized light (PL); (B) karst-filling giant calcite crystals at 5683.9 m in Well S75. $O_{1\text{-}2y}$; (C) type II fracture-filling calcite cross-cut by type III calcite and type II karst-filling giant calcite crystal, S65, 5732.24 m, $O_{1\text{-}2y}$, PL; (D) the same view as (C), CL; (E) type II fracture-filling calcite, S65, 5733.21 m, $O_{1\text{-}2y}$, PL; (F) the same view as (E), CL; (G) type I karst-filling giant calcite crystals, well S65, 5475.59 m, $O_{1\text{-}2y}$, PL; (H) the same view as (G), CL; (I) four zones of type II karst-filling giant calcite crystal, S75, 5735.6 m, $O_{1\text{-}2y}$, PL; (J) the same view as (I), S75, 5735.6 m, $O_{1\text{-}2y}$, CL; (K) barite cross-cuts type II karst-filling giant calcite crystal, S110, O_{2yj}, 6258 m, cross-polarized light; (L) large oil fluid inclusions in barite, well S110, O_{2yj}, 6258 m, PL; (M) different generations of calcite cements, T751, O_{2yj}, 5839.14 m, PL; (N) the same view as (C), CL.

crosscut by type III (Fig. 4C,D). Type I fracture-filling calcite occurs as fine crystals and type II and type III fracture-filling as fine to coarse euhedral crystals. Under cathodoluminescence (CL), type I calcite is dull red, type II calcite is nonluminescent and has a Mn content of 89 μg g^{-1} and Fe of 300 μg g^{-1} in well S65 (Tables 2 and 3), and type III calcite is dull red with Mn of 106 μg g^{-1} and Fe 200 μg g^{-1} in well S76 (Fig. 4C–F).

Karst-filling calcite is calcite that has grown in a palaeocave with a diameter more than 6 to 15 mm (Ford & Ewers 1978); it shows giant forms with crystal sizes from about 1–5 mm (Fig. 4B) and were found in the Lower to Middle Ordovician from wells S65, S72, S75, and S85 with a thickness up to 6 m. The calcites have two different CL responses: nonluminescent CL in wells S65 and S75 with Mn from 83 to 91 μg g^{-1} ($n = 2$, Table 2) and Fe from 400 to 700 μg g^{-1}, and dull red – orange yellow CL in wells S72, S78, and S85 with Mn 232 μg g^{-1} and Fe from 498 to 797 μg g^{-1} (Fig. 4C,D,G–J).

Barite occurs as tabular, vug-fillings, and crosscuts karst-filling giant calcite crystals (Fig. 4K).

Interparticle calcite cements are present in three stages. Stage I-1 calcite is cloudy, fibrous or radiaxial fibrous and nonluminescent (Fig. 4M,N); this type of calcite has been reported from normal marine diagenetic environments (Moore 2001). Stage I-2 calcite is bladed and granular and red to orange yellow CL colors (Fig. 4O,P). Stage I-1 calcite was infrequently followed by stage I-2 calcites. Stage II occurs as blocky crystals (>0.1 mm) in the center of pores and dull red CL (Fig. 4O,P). Stage III calcite occurs as coarse crystals and is nonluminescent under CL.

Table 2 Mn and Fe contents of different calcites.

Well	Formation	Depth (m)	Occurrence	Mn (μg g^{-1})	Fe (μg g^{-1})
S65	$O_{1\text{-}2}y$	5733.21	Frac. Cc-2	89	300
S76	$O_{1\text{-}2}y$	5744.8	Frac. Cc-3	106	200
S85	$O_{1\text{-}2}y$	5964.6	Frac. Cc-1	232	498
S78	$O_{1\text{-}2}y$	5329.2	Karst Cc-1	232	797
S65	$O_{1\text{-}2}y$	5532.79	Karst Cc-2	83	700
S65	$O_{1\text{-}2}y$	5732.24	Karst Cc-2	91	400

Homogenization temperature (HT) and salinity

Seventeen samples were doubly polished and analyzed for fluid inclusions. Abundant fluid inclusions were observed in fracture-, karst-fillings and calcite cements (collectively called diagenetic calcite). Most of the inclusions occur in planar arrays along growth banding and appear to be primary and therefore were probably trapped during primary crystal growth of the minerals. Some of the inclusions are distributed across CL-defined growth banding and thus are secondary. Although some monophase, liquid aqueous inclusions were observed in type I fracture-filling calcite and late calcite fluid-inclusion assemblages (FIAs), most of the fluid inclusions are 2-phase aqueous vapor–liquid. In the following section, only aqueous 2-phase primary inclusions were measured for homogenization temperatures and salinities.

The type I fracture-filling calcite contains a few fluid inclusions. The fluid inclusions occur mainly as single-phase aqueous inclusions and have sizes <4 μm in general, which are too small to be measured for salinities. Small proportions of the fluid inclusions occur as aqueous 2-phase inclusions and have homogenization temperatures ranging from 57 to 83.4°C ($n = 9$). None of the fluid inclusions show UV fluorescence revealing that there was no petroleum present at the time these cements grew.

Type II fracture-filling calcite contains abundant single-phase aqueous and vapor–liquid 2-phase fluid inclusions. The latter fluid inclusions have low vapor to liquid ratios (<15%) and homogenization temperatures from 105.8 to 178.7°C ($n = 25$) and salinities from 4.0 to 10.9 wt% NaCl equiv ($n = 8$). A small fraction of the fluid inclusions show orange to yellow UV fluorescence emission colors

Table 3 Sr contents, $^{87}Sr/^{86}Sr$, homogenization temperatures and salinities of fluid inclusions and CL colors of different cements.

Cements	Sr contents (μg g^{-1})	$^{87}Sr/^{86}Sr$	Homogenization temperatures (°C)	Salinities (wt% equiv. NaCl)	CL colors
Frac. Cc-1	59.2–99.9	0.7087–0.7096	57–83.4	–*	Dull red
Frac. Cc -2	204.3–648.9	0.7090–0.7099	105.8–178.7	4.0–10.9	Nonluminescent
Frac. Cc -3	111.2-158.5	0.7090–0.7096	63.4–121.1	3.7–8.6	Dull red to orange yellow
Karst Cc-1	101.0–151.0	0.7091–0.7099	65.9–117.7	3.2–9.0	Dull red to orange yellow
Karst Cc -2	223.8–1091.0	0.7091–0.7097	110.2–187.1	0.5–9.5	Nonluminescent
Cement -1-1	–*	–*	–*	–*	Nonluminescent
Cement -1-2	–*	–*	<50†	–*	Red to orange yellow
Cement -2	59.5	–*	57–107.9	3.6–7.2	Nonluminescent
Cement -3	161.5	–*	134.6–198.9	3.7–11.5	Nonluminescent
Barite	–*	–*	120–154	15.0–22.4	–*
Fluorite	–*	–*	84–116	18.6–20	–*

*No measurement available.
†From all-liquid fluid inclusions.

suggesting that some low to moderate maturity oil was present at the time these minerals grew.

Type III fracture-filling calcite contains only a few fluid inclusions, dominated by vapor-liquid 2-phase fluid inclusions with some gas-phase fluid inclusions. The fluid inclusions have regular shapes and show higher vapor to liquid ratios (20–30%) and homogenization temperatures from 63.4 to 121.1°C (n = 30), and salinities from 3.7 to 8.6 wt% NaCl equiv (n = 5). Associated with 2-phase aqueous inclusions are abundant oil inclusions, which have yellow to blue-white UV fluorescence emission colors.

Karst-filling, giant calcite crystal with dull red to orange yellow CL contains abundant monophase, liquid fluid inclusions and small amounts of 2-phase aqueous fluid inclusions with regular to irregular shapes. Oil-filled fluid inclusions were only rarely observed and showed orange to yellow UV fluorescence. The calcite shows a wide homogenization temperature range between 65.9 and 117.7°C (n = 49, Fig. 5) and wide salinities from 3.4 to 9.0 wt% NaCl equiv.

Nonluminescent karst-filling calcite contains less abundant fluid inclusions. The fluid inclusions are regularly shaped and dominated by 2-phase aqueous fluid inclusions with vapor to liquid ratios from 5% to 40% and have homogenization temperatures from 110.2 to 187.1°C (n = 60, Fig. 5) and salinities from 4.2 to 9.5 wt% NaCl equiv (n = 35, Fig. 4). The fluid inclusions are closely associated with abundant petroleum fluid inclusions with yellow to blue-white UV fluorescence emission colors.

Karst-filling, giant calcites in the Lower Ordovician in well S75 show four growth zones:

(1) Aqueous fluid inclusions in the innermost zone have a vapor to liquid ratio of <15%, sizes of 3 to 11 μm, homogenization temperatures mainly from 123 to 140°C (n = 7), and salinities from 1.4 to 9.2% (n = 5).
(2) Aqueous fluid inclusions in the second zone are abundant and have sizes from 3 to 14 μm, vapor to liquid ratio <15% in general, homogenization temperatures from 148 to 160°C, and salinities from 0.7 to 5.0 wt% NaCl (n = 5).

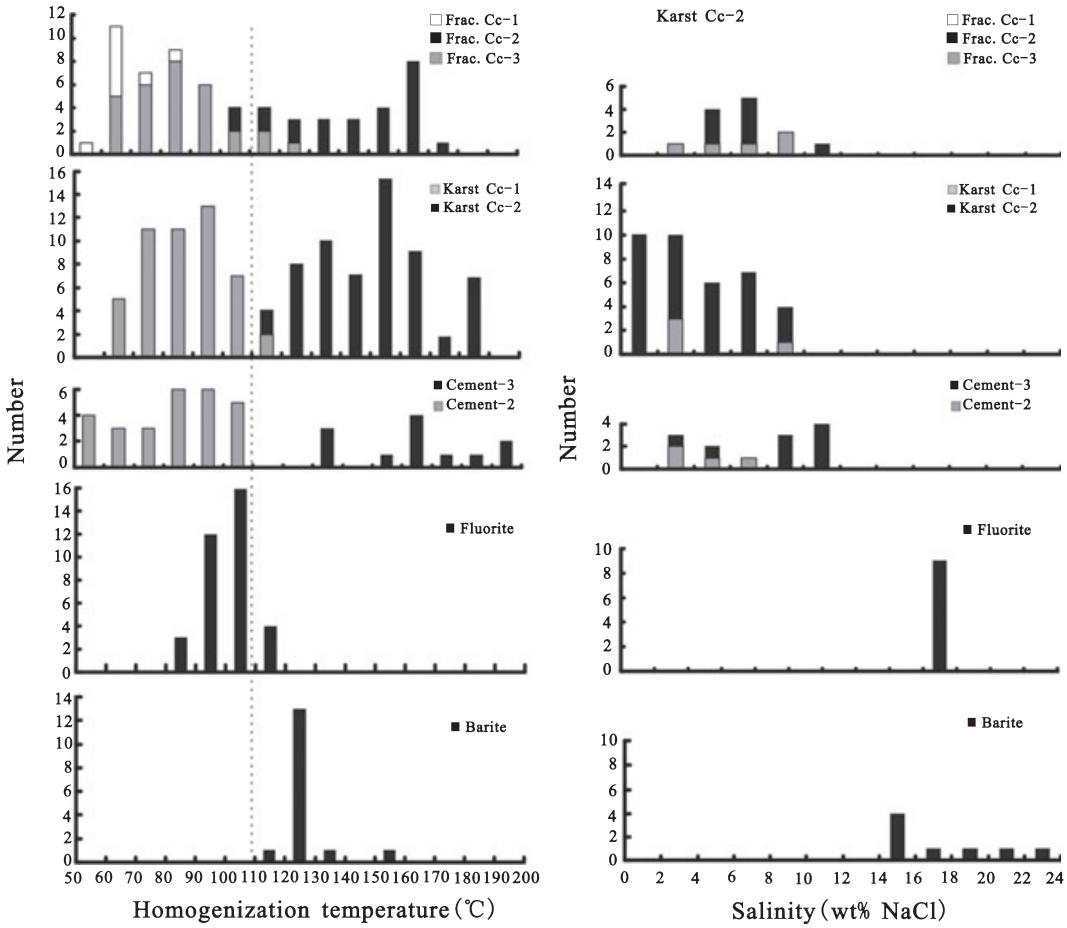

Fig. 5. Histograms showing homogenization temperatures and salinities measured from fluid inclusions of fracture-, karst- and interparticle cement from the Ordovician.

(3) Aqueous fluid inclusions in the third zone are dominated by 2-phase vapor–liquid fluid inclusions with small numbers of gas-phase fluid inclusions. Most of the fluid inclusions have vapor to liquid ratios <15% and 3 to 14 μm in size. The fluid inclusions have a wide range of homogenization temperatures from 117 to 140°C (n = 10) and salinities from 0.5 to 3.4 wt% NaCl (n = 4).
(4) Aqueous fluid inclusions in the outermost zone have sizes from 3 to 6 μm. Most of the fluid inclusions are all-liquid and only a few occur as gas–liquid fluid inclusions. The vapor–liquid fluid inclusions have homogenization temperatures from 165 to 180°C (n = 3) and salinities from 0.7 to 1.2 wt% NaCl (n = 4).

Giant form calcite from innermost zone to outer zone in well S75 have homogenization temperatures varying from 123 to 140°C, 148 to 160°C to 117 to 140°C, and salinities mostly less than present seawater (3.5 wt%).

No measurable fluid inclusions were observed in stage 1–1 and 1–2 calcite cements (Cement 1–1 and Cement 1–2). Fluid inclusions in stage II calcite cements (Cement-2) have sizes from 4 to 10 μm, and show homogenization temperatures from 57 to 107.9°C (n = 27) and salinities from 3.6 to 7.2 wt% NaCl (n = 7). Stage III cements (Cement-3) show high homogenization temperatures from 134.6 to 198.9°C (n = 12) and salinities from 3.7 to 11.5 wt% NaCl (n = 9) (Fig. 4, Table 3).

Large oil inclusions (up to 50 μm) are ubiquitous in barite (Fig. 4I) and only a few small aqueous vapor–liquid inclusions are present. Barite shows a narrow homogenization temperature range from 120 to 154°C (n = 14) and salinities from 15.0 to 22.4 wt% NaCl (n = 8) (Fig. 5). Coexisting with barite is fluorite with homogenization temperatures of 84–116°C and salinities of 18.6–20.0 wt% (n = 6).

Relationship between homogenization temperatures and salinities of fluid inclusions show that an increase in homogenization temperatures and salinities from Karst Cc-1 and Frac. Cc-3, cement -2 to fluorite and barite. Frac. Cc-2, cement -3 and Karst Cc-2 have a similarly wide homogenization temperatures range, but Karst Cc-2 show significantly lower salinities (<3.5 wt%) than Frac. Cc-2 and cement -3 (Fig. 6).

Sr, $^{87}Sr/^{86}Sr$, $\delta^{18}O$ and $\delta^{13}C$ of fracture-fillings

The trace element and isotopic compositions of the calcite are listed in Table 4. Twenty fracture-filling calcite crystals and karst-filling giant calcite crystals from the Ordovician have $^{87}Sr/^{86}Sr$ ratios from 0.7085 to 0.7099, most of which are significantly higher than bulk carbonate and contemporary seawater $^{87}Sr/^{86}Sr$ ratios (0.7060–0.7090) (Fig. 7).

Type I fracture-filling calcite has low Sr contents from 59.2 to 111.1 μg g^{-1} (n = 4) and low Ba, Pb, and Zn contents. Type II fracture-filling calcite has Sr content varying between 92.6 and 648.9 μg g^{-1} (n = 8) and Ba contents up to 12760 μg g^{-1}. Karst-filling, giant form calcite has Sr contents mainly from 101 to 244 μg g^{-1} with a maximum of 1091 μg g^{-1} (n = 6). Two calcite cement samples have Sr contents of 59.5 μg g^{-1} and 161.5 μg g^{-1}, respectively.

Most of the diagenetic calcite samples show more negative carbon isotopes (as low as −8.3‰) than bulk carbonates in the Ordovician in the basin (Jiang *et al.* 2001). Giant form calcite from well T417 has light $\delta^{13}C$ values (−3.7‰ and −5.9‰) and light $\delta^{18}O$ values at about −11.0‰ (n = 2). These values are close to the −1.7 to −5.1‰ for $\delta^{13}C$ values and −13.7 to −16.6‰ for $\delta^{18}O$ values of giant calcite from well S85, respectively (Qian *et al.* 2009). $\delta^{18}O$ values for the calcites range from −8.3‰ to −16.8‰. There is a positive correlation between $\delta^{13}C$ and $\delta^{18}O$ values (Fig. 8A) and negative correlation relationships of $^{87}Sr/^{86}Sr$ ratios to $\delta^{18}O$ and $\delta^{13}C$ values for the calcite (Fig. 8A).

Chemistry, $\delta^{13}C_{HCO_3^-}$ and $^{87}Sr/^{86}Sr$ of formation water

Total dissolved solids (TDS) of formation waters in the Tabei area range from 61 000 to 297 200 mg l^{-1}.

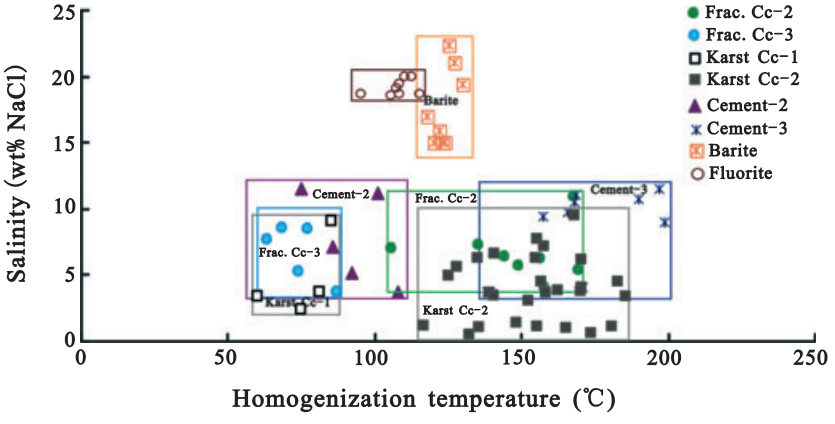

Fig. 6. Relationship between homogenization temperatures and salinities of the fluid inclusions from diagenetic calcite, fluorite, and barite.

Table 4 Trace elements contents, and Sr, C and O isotopic compositions of fracture- and Karst-filling calcite and cement.

Sample Number	Well	Formation	Depth (m)	Sample Occurrence	Zn (μg g^{-1})	Sr (μg g^{-1})	Ba (μg g^{-1})	Pb (μg g^{-1})	$\delta^{13}C$ (‰)	$\delta^{18}O$ (‰)	$^{87}Sr/^{86}Sr$
1	S106-4	O_2yj	6001.5	Frac. Cc-1	2.16	111.18	13.25	0.82	−3.21	−12.77	0.70936
2	T709	$O_{1\text{-}2}y$	6149.5	Frac. Cc-1	−*	–	–	–	–	–	0.70871
3	T709	O_2yj	5940.27	Frac. Cc-1	2.14	99.53	28.04	0.56	−4.26	−14.17	0.70938
4	T739	O_2yj	6141	Frac. Cc-1	2.15	59.21	11.244	0.23	–	–	–
5	T904	O_3l	5777.63	Frac. Cc-1	5.99	99.93	26.90	0.64	–	–	0.70959
6	S14	$O_{1\text{-}2}y$	5407.01	Frac. Cc-2	8.51	414.37	65.83	0.90	−5.36	−14.91	0.70932
7	S47	$O_{1\text{-}2}y$	5462.9	Frac. Cc-2	4.88	158.51	44.02	1.19	−0.84	−9.48	0.70900
8	S47	$O_{1\text{-}2}y$	5462.9	Frac. Cc-2	5.52	351.87	367.88	1.11	−2.27	−9.82	0.70904
9	S77	$O_{1\text{-}2}y$	5443.25	Frac. Cc-2	11.84	648.90	12759.79	1.14	−1.29	−11.62	0.70972
10	S81	$O_{1\text{-}2}y$	5710.33	Frac. Cc-2	2.28	204.35	12.04	0.80	−1.82	−16.82	0.70993
11	S86	$O_{1\text{-}2}y$	5701.27	Frac. Cc-2	–	–	–	–	−8.25	−12.66	0.70951
12	S88	O_1p	6456.27	Frac. Cc-2	1.39	382.06	8.69	0.49	–	–	0.70899
13	S106-4	O_2yj	6001.65	Frac. Cc-3	1.26	92.61	12.94	0.37	−3.21	−13.44	0.70940
14	T204	$O_{1\text{-}2}y$	5560.1	Frac. Cc-2	–	–	–	–	−1.04	−8.31	0.70851
15	T904	O_3l	5777.63	Frac. Cc-3	2.24	126.22	16.78	0.62	−2.96	−12.28	0.70959
16	S47	$O_{1\text{-}2}y$	5462.98	Karst Cc-1	3.99	150.96	45.37	0.71	−1.58	−9.40	0.70912
17	S110	O_3l	6086.71	Karst Cc-2	9.97	1090.98	18518.91	0.65	–	–	0.70967
18	T417	$O_{1\text{-}2}y$	5506.92	Karst Cc-2	2.36	243.66	65.49	0.95	−5.9	−11	0.70924
19	T417	$O_{1\text{-}2}y$	5598.05	Karst Cc-2	1.86	223.83	187.53	1.07	−3.7	−10.9	0.70918
20	T904	O_2yj	5894.56	Karst Cc-1	2.97	101.02	421.31	0.47	–	–	0.70990
21	T904	O_3l	5773.66	Karst Cc-1	3.05	124.54	2187.75	1.89	–	–	0.70920
22	S88	$O_{1\text{-}2}y$	6159.8	Cement-3	3.41	161.48	16.66	0.66	–	–	–
23	T739	O_2yj	6141	Cement-2	1.79	59.47	10.74	0.28	–	–	–

*No measurement.
Frac. Cc represents fracture-filling calcite; Karst Cc represents karst-filling giant crystalline calcite.

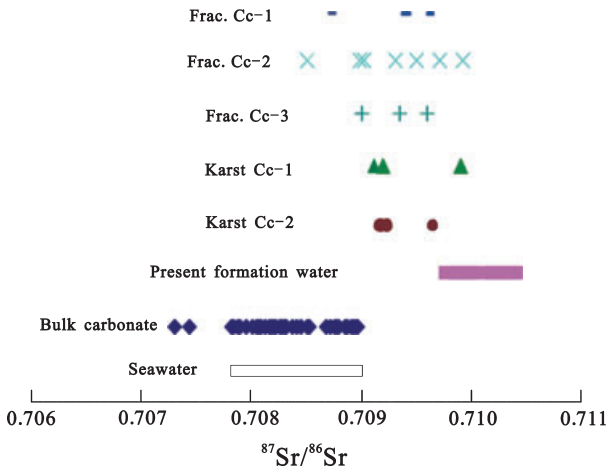

Fig. 7. $^{87}Sr/^{86}Sr$ ratios of fracture-, and karst-filling calcite and present formation waters in comparison with bulk carbonate rocks in the Ordovician (Jiang *et al.* 2001) and seawater of Ordovician age (Burke *et al.* 1982).

Formation waters with relatively high TDS occur mainly in the areas of wells S67-S79-S65-T601-S88-S85 and T204-T205-TS1 (>160 000 mg l^{-1}) in the southwest of the Tabei area, and low TDS waters are mostly present in Lunnan area (<160 000 mg l^{-1}) in the northeast (palaeohighs) (Fig. 9).

$^{87}Sr/^{86}Sr$ ratios of twenty-four water samples measured range from 0.7098 to 0.7104, with an average of 0.7101 (Jia *et al.* 2007). The ratios are slightly higher than those of fracture- and karst-filling calcites and are significantly higher than those of bulk carbonate rocks (Jiang *et al.* 2001) and coeval seawater (Burke *et al.* 1982) (Fig. 7). The formation waters have higher $^{87}Sr/^{86}Sr$ ratios in the wells in the west than in the east of the Tahe area (not shown).

$\delta^{13}C_{HCO_3^-}$ values of the 24 formation water samples range from −6‰ to −13.8‰. The $\delta^{13}C_{HCO_3^-}$ values of the water samples from different wells shows that, $\delta^{13}C_{HCO_3^-}$ values become less negative from the west to the east in general (not shown). Similar to calcite samples, there is a linear positive correlation relationship between $\delta^{13}C$ and $\delta^{18}O$ values and a negative relationship between $^{87}Sr/^{86}Sr$ ratios and $\delta^{13}C_{HCO_3^-}$ values for the water samples (Fig. 8B).

DISCUSSION

Re-equilibration of fluid inclusions during subsequent heating events?

Several investigators (e.g. Goldstein 1986; Burruss 1987; Prezbindowski & Larese 1987) have suggested that homogenization temperatures of fluid inclusions in carbonates (specifically calcite) can be affected by re-equilibration during later heating events. Their studies indicate that re-equilibration may cause aqueous inclusions to yield a

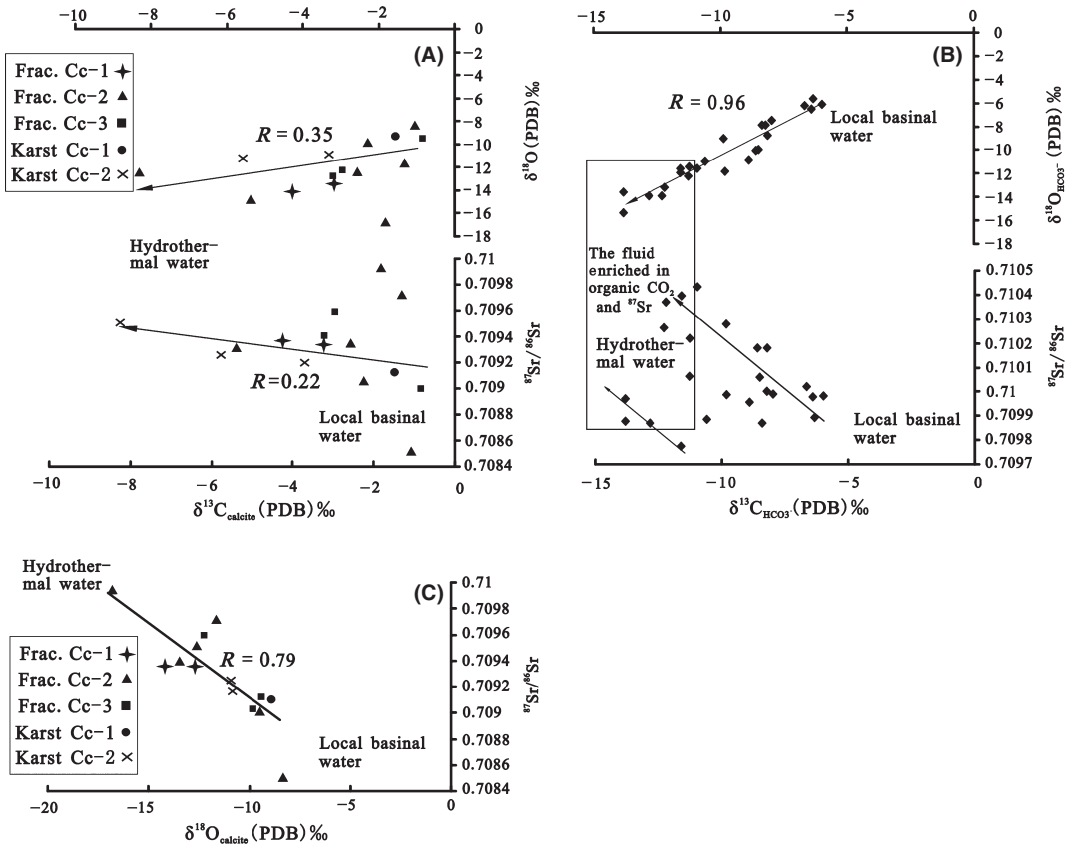

Fig. 8. Cross plots showing, (A) the relationships of $\delta^{13}C$ values to $\delta^{18}O$ values and $^{87}Sr/^{86}Sr$ ratios for 11 fracture-filling calcite and two giant calcite crystals in this study; (B) variations of $\delta^{13}C$, $\delta^{18}O$ and $^{87}Sr/^{86}Sr$ for 24 formation water samples (data from Jia *et al.* (2007)); and (C) the relationship between $\delta^{18}O$ values and $^{87}Sr/^{86}Sr$ ratios for diagenetic calcite.

poor record of their low-temperature history, but a useful record of the maximum temperature experienced by the host rock (Burruss 1987).

In the Tahe oilfield, most of the fluid inclusions are likely not re-equilibrated from existing inclusions caused by stretching when crystal growth and fluid inclusion assemblages are considered. This proposal is supported by the following lines of evidence on the basis of criterions of Goldstein & Reynolds (1994) and Worden *et al.* (1995) (i) most of the fluid inclusions have sizes in a narrow range and are small, mainly from 4 to 13 μm, (ii) no obvious correlation was observed between the size of an inclusion and its homogenization temperature, (iii) in giant calcite crystals from well S75, the inclusions can be segregated petrographically into different fluid-inclusion assemblages that each have different homogenization temperature ranges. HT ranges in the innermost zone and second zone are less than 15°C and thus are considered to be consistent (Goldstein & Reynolds 1994). A slightly wider homogenization temperature range in the third zone (117–140°C) may indicate that precipitation of this calcite occurred over the temperature range rather than re-equilibration of the inclusions when consistent homogenization temperature data are considered for fluid-inclusion assemblages from the innermost and second zones (Goldstein & Reynolds 1994). Fluid inclusions in the outermost zone may have resulted from necking down. This is supported by two lines of evidence, (i) the fluid inclusions have significantly smaller sizes in this zone than in the other zones, and (ii) vapor–liquid 2-phase fluid inclusions with significantly higher homogenization temperatures (165–180°C) than those in other zones (123–160°C); however, the 2-phase fluid inclusions in the outermost zone coexist with monophase liquid fluid inclusions that are considered to have homogenization temperatures lower than 50°C (Goldstein & Reynolds 1994), and thus, homogenization temperatures in this zone are considered to be inconsistent (Goldstein & Reynolds 1994). Fluid inclusions in the outermost zone are ruled out for further discussion.

Origin of ^{12}C- and ^{87}Sr-rich water

Almost all of the $^{87}Sr/^{86}Sr$ measurements from brines and diagenetic calcite in the Tahe oilfield are higher than those of the Ordovician limestone and underlying Cambrian dolomite in the basin. This evidence indicates that

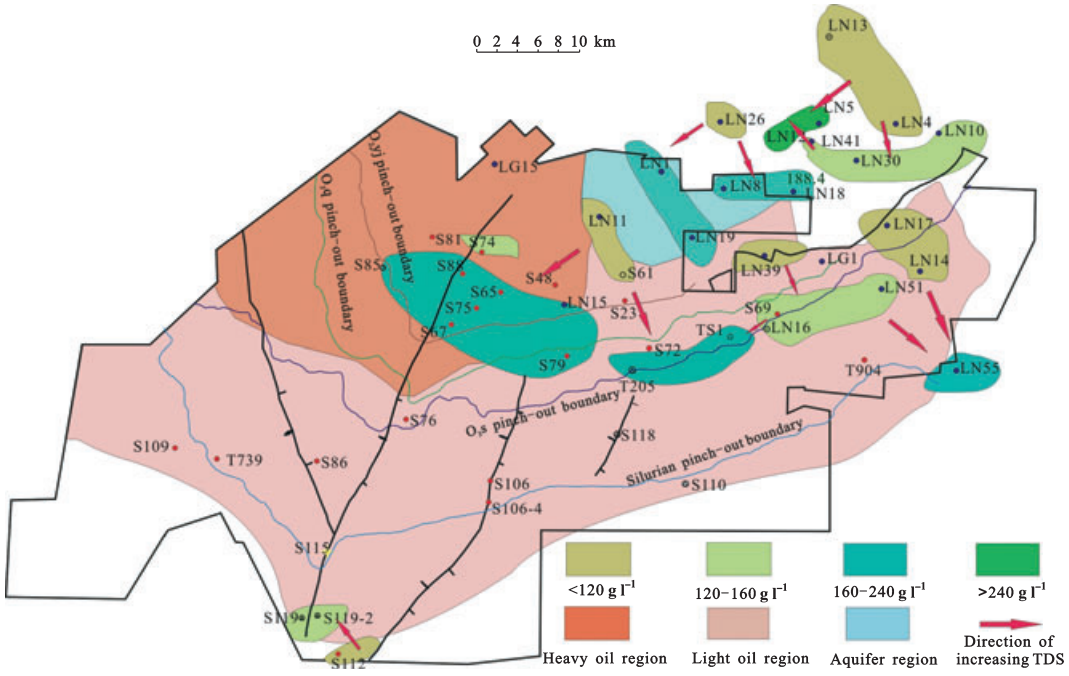

Fig. 9. Mapped present formation water total dissolved solids (TDS, in g l^{-1}) for the Ordovician with the distribution of different types of oils and water.

radiogenic Sr may have been derived from continental aluminosilicates, but not from carbonates *in situ*. ^{87}Sr-rich water may have been derived from meteoric water which infiltrated the clastic rock in the surface, or from hyperthermal water which obtained ^{87}Sr from the deeper strata in the basin.

^{12}C-rich HCO_3^- may have a similar source to the radiogenic Sr as indicated by the negative correlation relationship between $^{87}Sr/^{86}Sr$ ratios and $\delta^{13}C$ values of diagenetic calcite and formation waters. Isotopically light carbon in Frac. Cc-2 calcite (down to −8.3‰) and formation water (−6.0‰ to −13.8‰) were most likely derived from oxidization of organic matter (OM, i.e. petroleum and/or kerogen), perhaps by thermochemical sulfate reduction (TSR), and less likely from meteoric diagenetic environments. $\delta^{13}C$ values of meteoric diagenetic fluids are determined by the ratios of the amount of dissolved limestone and the amount of carbon from soil gas and have been shown to range from −11 to +1‰; the calcites precipitated from these fluids have $\delta^{13}C$ values of −10 to +2‰ (Allan & Mathews 1982). These calcites show constant $\delta^{18}O$ and variable $\delta^{13}C$ values (Lohmann 1988). In the case of the Tahe area, (i) some of the formation waters have $\delta^{13}C_{HCO_3^-}$ values lighter than those of the meteoric diagenetic fluids; (ii) the calcites analyzed do not show constant $\delta^{18}O$ values relative to their $\delta^{13}C$ values; and (iii) salinities of Frac. Cc-2 calcite with the lightest carbon range from 4.0 to 10.0 wt%, and salinities of the formation waters range from 142 530 mg l^{-1} to 232 430 mg l^{-1} with an average of 214 780 mg l^{-1} (n = 20); these salinities are significantly higher than modern seawater (3.5 wt%). All these three lines of evidence argue against a source of isotopically light carbon coming mainly from meteoric digenetic fluids. In contrast, isotopically light carbon may have been derived from organic mater oxidation possibly by TSR (Cai *et al.* 2003, 2004). That is, ^{87}Sr-rich water has been derived from the area where OM was oxidized, or OM was oxidized during the flow of ^{87}Sr-rich water.

The ^{87}Sr-rich water may have experienced high temperatures, as indicated by the fact that some calcite with high $^{87}Sr/^{86}Sr$ ratios shows very light $\delta^{18}O$ values. Calcite with light $\delta^{18}O$ values may have precipitated either from low temperatures and meteoric water environment, or from an environment with relatively high temperatures and heavier $\delta^{18}O$ values. Palaeo-meteoric water has been shown to have heavier $\delta^{18}O$ and δD values than present surface water as typified by Kongque River (δD = −72‰, $\delta^{18}O$ = −11.5‰; Cai 2000; Cai *et al.* 2001a). For example, meteoric water of Devonian age was shown to have a $\delta^{18}O$ value of −5.5‰ and δD of −35‰ in the Tarim Basin (Cai *et al.* 2001a). The latitude of the Tarim area during the Paleozoic has been shown to be less than 30°N, which are lower than present-day latitude of 41.5°N (Fang *et al.* 1996). Thus, oxygen isotope values of freshwater of Permian age (Hercynian orogeny) can be estimated to be less negative than −9.2‰ PDB (or 14.6‰ SMOW) (Cai 2000). It is unlikely for relatively light $\delta^{18}O$ values (down to −16.8‰ PDB or 13.6‰ SMOW) of calcite to have been derived from the meteoric water of Permian age with temperatures <50°C, based on the oxygen isotope

equilibrium fractionation equation between calcite and pure water: $1000 \ln\alpha = 2.78\times10^6/T^2 - 2.89$ (O'Neil *et al.* 1969) (Fig. 10). This line of argument suggests that at least some of the isotopically light oxygen in diagenetic calcite may have been derived from relatively high-temperature water.

Thus, enrichment in radiogenic Sr, light oxygen isotopes in some present formation water and palaeo-water may have been derived from relatively high-temperature interaction with aluminosilicates in deeper strata.

Isotopically light carbon measured from formation water and some calcite with homogenization temperatures higher than 120°C is most likely derived from TSR by petroleum in deeper strata in this area, as initially proposed by Cai *et al.* (2009), who has provided supporting evidence, including high H_2S contents in gas composition and gaseous phase fluid inclusions and heavy $\delta^{34}S$ values (25–29‰) of fracture-filling pyrite and oils. However, no direct evidence indicates the isotopically light carbon and heavy sulfur are genetically linked; thus, the possibility that isotopically light carbon may have been directly derived from kerogen cracking cannot be ruled out.

Water mixing and cross-formation flow

Previous studies (Cai *et al.* 1997 and Jia *et al.* 2007) have shown that there is mixing between meteoric water and basinal water in the Tabei area, based on the relationship between δD and $\delta^{18}O$ values.

In this study, basinal water *in situ* or diagenetically altered connate water (Fisher & Boles 1990) is indicated by its $^{87}Sr/^{86}Sr$ ratios from 0.7085 to 0.7090 inferred from two fracture-filling calcites (Table 4).

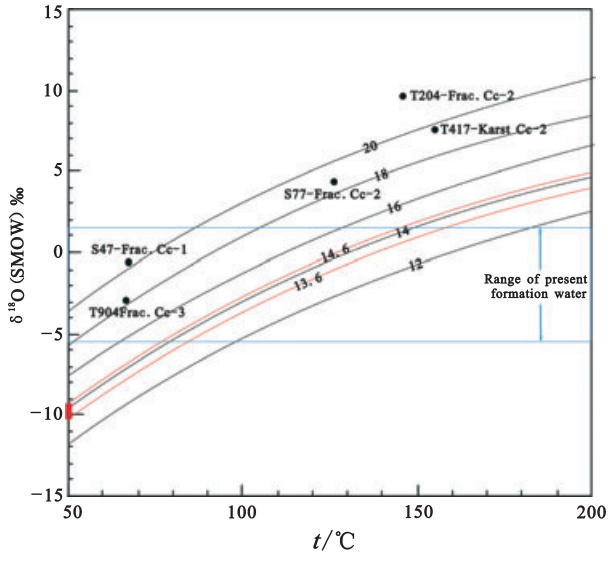

Fig. 10. Cross plot of diagenetic water oxygen isotopes versus homogenization temperature of aqueous inclusions of calcites.

A meteoric water end-member is indicated by three lines of evidence:

(1) high $^{87}Sr/^{86}Sr$ ratio but low Sr concentration (Table 4),
(2) low salinities (<3.5 wt% NaCl) in fluid inclusions in karst-filling giant calcite crystals (Karst Cc-1),
(3) precipitation temperatures below 50°C as inferred from all-liquid fluid inclusions (Goldstein & Reynolds 1994),
(4) generally low Sr, Ba, and Zn concentrations in type I fracture-filling calcite.

Hydrothermal calcite and barite are indicated by their homogenization temperatures about 5–20°C higher than what experienced by the carbonates as indicated by burial and thermal history in well S109 in the south and well S75 in the north (Fig. 2) (e.g. Machel & Lonnee 2002; Cai *et al.* 2008). Barite, stage III calcite cements, and part of type II fracture-fillings and karst-filling, giant calcite crystals have homogenization temperatures higher than 120°C in the Ordovician in the Tahe area, which were measured on nonreequilibriated or non-necked-down fluid inclusions as discussed in re-equilibration of fluid inclusions during subsequent heating events?

Hydrothermal calcite is rich in ^{87}Sr with $^{87}Sr/^{86}Sr$ ratios up to 0.7097 and Sr concentrations up to 1091 μg g^{-1} in well S110 in the south. Thus, the hydrothermal water must have obtained radioactive Sr as well as Ba and Zn from deeper strata by interacting with ^{87}Sr-rich minerals or detrital rocks.

Different from hydrothermal calcite in the south, fluid inclusions of some hydrothermal calcite from wells S75 and S65 in the north are shown to have low salinities but high homogenization temperatures, similar to fluid inclusions from wells S85 and S79 in this area (Qian *et al.* 2009). Fluid inclusions with high temperatures (120 to 187°C) and low salinities (about 5 wt% equiv. NaCl) were also reported from epigenetic dolomites in southeast Missouri (Shelton *et al.* 1992). This kind of calcite may have precipitated from a variety of processes:

(1) Deeply recycled meteoric water,
(2) Mixing of meteoric water with hydrothermal water,
(3) Thermochemical sulfate reduction.

Deeply recycled water, i.e. meteoric water, could have flowed down along faults to deep strata and thus became significantly heated. Subsequently, the heated meteoric water underwent upward migration and led to the precipitation of hydrothermal calcite. This model of water flow was previously proposed by Qing & Mountjoy (1992) to explain variation of homogenization temperatures, $^{87}Sr/^{86}Sr$ and $\delta^{18}O$ values from saddle dolomite cements from the west toward the east in Western Canada sedimentary basin as a result of tectonic thrusting and compression, sedimentary loading, and tectonic uplift on the western margin. The structural history of the Western Canada basin is broadly analogous to that of the Tahe area; thus, it is

possible for similar model of water flow to have occurred in the two areas.

Alternatively, the hydrothermal calcite in the north may have precipitated from meteoric water mixed with hydrothermal fluids. Reservoirs in the north were covered directly by Carboniferous sediment and must have been infiltrated and thus dissolved by palaeo-meteoric water to some degree, resulting in the formation of karst which was subsequently connected by fractures to form networks (Zhang & Wang 2004; Jing *et al.* 2005; Qian *et al.* 2009). Similar karst reservoirs have been reported from around the world (Lohmann 1988; Lucia 1995; Louks 1999; Moore 2001); however, some of the cases have been debated and re-explained as a result of hydrothermal water activity (Qing & Mountjoy 1994; Davies & Smith 2006).

The karstic voids may have been full of meteoric water. Present oils in the Tahe oilfield are produced mainly from reservoirs with karstic voids or vugs connected by fractures at 100–150 m (not more than 230 m) below the Carboniferous–Ordovician unconformity. In the south, Lower Ordovician reservoirs are covered by the Middle and Upper Ordovician and thus much less influenced by palaeo-meteoric water. Consequently, reservoirs in the south have much less karst and smaller amounts of palaeo-meteoric water; thus, the water after mixing with hydrothermal water is expected to have higher salinities in the south than in the north. However, if this model applies, fluid inclusions with highest temperatures are expected to have the highest salinities rather than lowest salinities as found in this area.

The third possibility is that hydrothermal calcite with high homogenization temperatures and low salinities may have precipitated from TSR – derived water. This proposal is supported by the occurrence of TSR in this area (Section Origin of ^{12}C- and ^{87}Sr-rich water) and generation of water during TSR as proposed by Worden *et al.* (1996). Because this kind of calcite has homogenization temperatures significantly higher than temperatures ambient rock experienced, it is possible for ^{87}Sr-rich hydrothermal water together with TSR-H_2S and CO_2 to have migrated from deeper strata. Alternatively, elevated temperatures from hydrothermal water activity resulted in TSR and the generation of TSR water in the Ordovician reservoirs. Further study on this aspect is needed.

Palaeo-water evolution

It has generally been demonstrated that inclusion oils of higher API gravity and maturity fluoresce in the blue end of the visible spectrum, whereas inclusion oils of lower API gravity and maturity fluoresce in the red region (Burruss *et al.* 1985; McLimans 1987; Bodnar 1990). Thus, visually determined fluorescence colors of inclusion oils, in combination with petrological observation, aqueous fluid-inclusion data and burial histories of the Tahe oilfield can be used to constrain the precipitation sequence of the diagenetic calcite, barite, and fluorite, as is summarized in Fig. 11. Diagenetic water in this area may have evolved as follows.

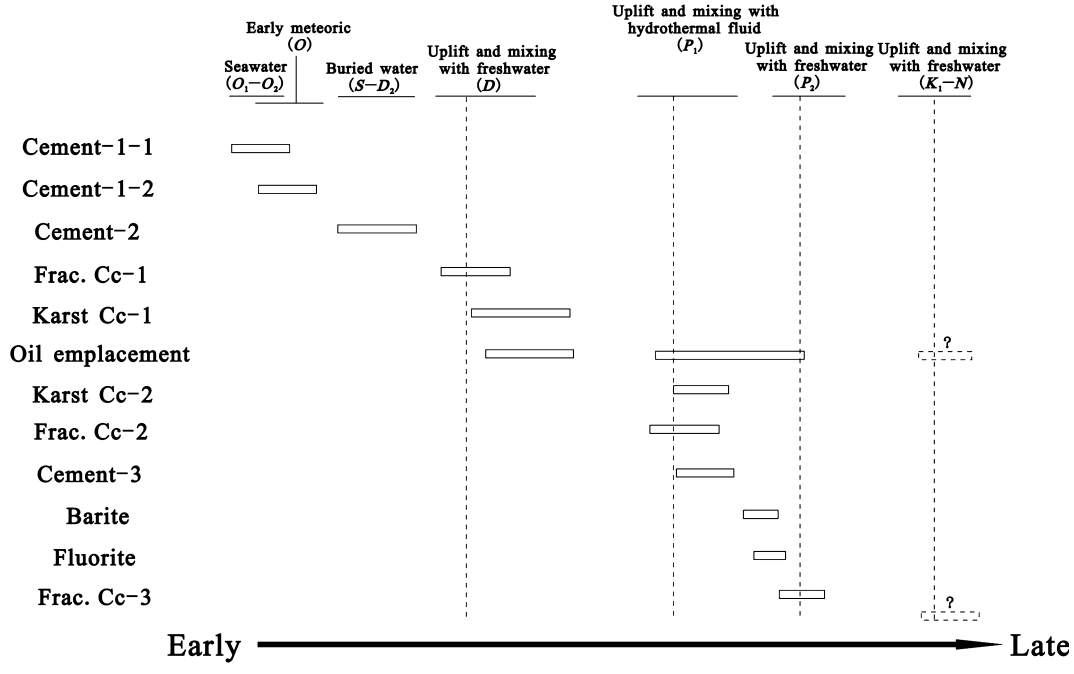

Fig. 11. Synthetic paragenetic sequence shows main stages in the diagenetic evolution of Ordovician carbonates.

The original water was seawater of Early to Middle Ordovician age, from which fibrous calcite precipitated (Cement 1-1). Subsequently, the sediments were exposed to vadose and phreatic zones and the water was diluted by meteoric water, from which bright CL (red to orange yellow) calcite (Cement 1-2) precipitated at <50°C under weak reducing environments (Muchez *et al.* 1998). During the Silurian to Middle Devonian, the sediments were buried to depths corresponding to temperatures from 57 to 110°C, the diagenetic environment became more reducing and thus more Fe(II) may have been released from minerals, resulting in an increase in Fe to Mn ratio in calcite cement. The calcite that precipitated from this burial environment (Cement-2) is nonluminescent under CL. During the late Caledonian Orogenies in the late Devonian, the carbonate rocks were uplifted, subsequently exposed to the surface and infiltrated by ground water, leading to significant dissolution of the carbonates and thus the formation of karst. The water in fractures and the karstic voids during this period had temperatures from <50 to 83°C, low salinities (<9.0 wt%), high Mn contents, and high $^{86}Sr/^{87}Sr$ ratios from 0.7090 to 0.7099, as measured from Frac. Cc-1 and Karst Cc-1. The low temperature water coexisted with lower maturity oils with orange to yellow UV fluorescence emission colors as recorded in Karst Cc-1 fluid inclusions.

Hydrothermal water may have entered the carbonate rocks during the early Permian, from which calcite cements (Frac. Cc-2 and Cement-3) and barite were precipitated at temperatures from 120 to 180°C and show significantly higher $^{86}Sr/^{87}Sr$ ratios and lighter $\delta^{13}C$ and $\delta^{18}O$ values. The hydrothermal water was accompanied by the emplacement of higher maturity oils with yellow to blue-white UV fluorescence emission colors as recorded in the barite. This feature suggests that the hydrothermal water has collected ^{87}Sr and oils of high maturity from Lower Cambrian and pre-Cambrian detrital rock. Hydrothermal water is tentatively considered to have salinities higher than 22.4 wt% and temperatures higher than 154°C, as indicated by fluid inclusions in barite crystals (Table 3). However, higher temperatures (up to 187°C) and much lower salinities (down to 0.5 wt%) measured from karst-filling giant calcite crystals (Karst Cc-2) may suggest that at least some hydrothermal water was deeply recycled meteoric water after being heated in deeper strata, or water generated from TSR during hydrothermal water activity. Nonluminescence under CL for these high-temperature minerals (Frac. Cc-2, Karst Cc-2 and Cement-3) suggests a reduced (possibly Fe-rich) water during this period. The reduced water coexisted with high mature oils with yellow to blue-white UV fluorescence emission colors. The chemical composition of the hydrothermal water is still to be defined.

Subsequently, the carbonates were uplifted during the late Permian, and meteoric water of this period may have infiltrated the carbonates as recorded in Frac. Cc-3 calcite with decreasing homogenization temperatures and salinities of fluid inclusions and increasing Mn to Fe ratio (dull red to orange yellow CL colors). Mixing with palaeometeoric water of this and/or later periods (Yanshanian to Himalayan orogenies, Cai *et al.* 2001a) to different extents may have resulted in large variations in salinity of the oilfield waters with the lowest value in palaeohighs. In the oilfield area, some present oilfield waters have TDS close to salinities of fluid inclusions of barite, suggesting that the oilfield waters are of hydrothermal origin with salinity mainly from underlying Cambrian and pre-Cambrian evaporites and detrital rocks, being similar to Ordovician oilfield waters from Central Tarim (Cai *et al.* 2001a).

CONCLUSIONS

(1) In the Tahe oilfield, analyses of present formation water, cements, fracture- and karst-fillings and fluid inclusion indicate mixing between three different types of water, that is, local basinal water or diagenetically altered connate water, hydrothermal water, and several episodes of meteoric water influx during development of numerous unconformities.

(2) Local basinal water is characterized by $^{87}Sr/^{86}Sr$ ratios of 0.7085 to 0.7090 inferred from two fracture-filling calcites, relatively heavy $\delta^{13}C_{HCO_3^-}$ and $\delta^{18}O$.

(3) Hydrothermal water was enriched in Ba, ^{87}Sr, and Zn had temperatures >154°C and salinities >22.4 wt% NaCl equivalent and may have been sourced from Cambrian and pre-Cambrian evaporites and detrital rocks and possibly entered the carbonate rocks during the early Permian.

(4) Mixing of the hydrothermal water with basinal water *in situ* may have resulted in the precipitation of calcite and barite with more radiogenic Sr, lighter carbon and oxygen, and higher Ba and Zn concentrations than bulk limestone.

(5) However, it is possible that the hydrothermal water was deeply recycled meteoric water that was heated in deeper strata, or water generated from TSR during hydrothermal water activity. The chemical composition of the hydrothermal water is still to be defined.

(6) The meteoric water was ^{87}Sr-rich but Ba- and Zn-depleted and may have infiltrated the carbonates during at least two periods (the late Devonian and the late Permian), as recorded in karst-filling giant crystalline calcite and type I fracture-filling calcite (D_3) and in type III fracture-filling calcite (P_2). These calcites show decreasing homogenization temperatures and salinities of fluid inclusions and increasing Mn to Fe ratio (dull red to orange yellow CL colors) compared to burial calcite (stage II calcite cement).

(7) Mixing of palaeometeoric waters of the two periods and later (perhaps of late Cretaceous to Neogene age) with hydrothermal water and local basinal water may have resulted in present-day oilfield water salinity variations.

ACKNOWLEDGEMENTS

This work is financially supported by State Key Lab of Petroleum Resources & Prospecting, China University of Petroleum and united foundation of NSFC and China's Petroleum Chemical Industry (grant no. 40839906). Comments from Professor R. H. Worden, Dr. P. C. Smalley and an anonymous reviewer were helpful in improving the quality of the manuscript.

REFERENCES

Allan JR, Mathews RK (1982) Isotope signatures associated with early meteoric diagenesis. *Sedimentology*, **29**, 797–817.

Bodnar RJ (1990) Petroleum migration in the Miocene Monterey Formation, California, USA: constraints from fluid-inclusion studies. *Mineralogical Magazine*, **54**, 295–304.

Bodnar RJ (1993) Revised equation and table for determining the freezing point depression of H2O-NaCl solutions. *Geochimica et Cosmochimica Acta* , **57**, 683–4.

Burke WH, Denison RE, Hetherington EA, Koepnick RB, Nelson HF, Otto JB (1982) Variation of seawater 87Sr/86Sr throughout Phanerozoic time. *Geology*, **10**, 516–9.

Burruss RC (1987) Diagenetic paleotemperatures from aqueous fluid inclusions: re-equilibration of inclusions in carbonate cements by burial heating. *Mineralogical Magazine*, **51**, 477–81.

Burruss RC, Cercone KR, Harris PM (1985) Timing of hydrocarbon migration: evidence from fluid inclusions in calcite cements, tectonics and burial history. In: *Carbonate Cements, Soc. Econ. Paleontol. Mineral. Spec. Publ.*, Vol. **26** (eds Schneidermann N, Harris PM), pp. 277–89. SEPM, Tulsa, OK.

Cai CF, 2000. Fluid geochemistry: fluid origin, flow and fluid-rock interaction and case studies from the Tarim Basin. PhD Dissertation, Institute of Geology and Geophysics, Chinese Academy of Sciences, Beijing.

Cai CF, Mei BW, Ma T, Chen CP, Li W, Liu CQ (1997) *Approach to Fluid-Rock Interaction in the Tarim Basin*. Geological Publishing House, Beijing, 155.

Cai CF, Franks S, Aagaard P (2001a) Origin and migration of brines from Paleozoic strata in Central Tarim, China: constraints from $^{87}Sr/^{86}Sr$, δD, $\delta^{18}O$ and water chemistry. *Applied Geochemistry*, **16**, 1269–84.

Cai CF, Hu W, Worden RH (2001b) Thermochemical sulphate reduction in Cambo-Ordovician carbonates in Central Tarim. *Marine and Petroleum Geology*, **18**, 729–41.

Cai CF, Worden RH, Bottrell SH, Wang LS, Yang CC (2003) Thermochemical sulphate reduction and the generation of hydrogen sulphide and thiols (mercaptans) in Triassic carbonate reservoirs from the Sichuan Basin, China. *Chemical Geology*, **202**, 39–57.

Cai CF, Xie ZY, Worden RH, Hu GY, Wang LS, He H (2004) Methane-dominated thermochemical sulphate reduction in the Triassic Feixianguan Formation East Sichuan Basin, China: towards prediction of fatal H_2S concentrations. *Marine and Petroleum Geology*, **21**, 1265–79.

Cai CF, Li KK, Li HT, Li M, Chen LX (2008) Evidence for cross formational hot brine flow from integrated $^{87}Sr/^{86}Sr$, REE and fluid inclusions of the Ordovician veins in Central Tarim, China. *Applied Geochemistry*, **23**, 2226–35.

Cai CF, Zhang CM, Cai LL, Wu GH, Jiang L, Xu ZM, Li KK, Ma AL, Chen LX (2009) Origins of Palaeozoic oils in the Tarim Basin: evidence from sulfur isotopes and biomarkers. *Chemical Geology*, **268**, 197–210.

Davies GR, Smith LB (2006) Structurally controlled hydrothermal dolomite reservoir facies: an overview. *American Association of Petroleum Geologists Bulletin*, **90**, 1641–90.

Fang D, Tan X, Jiang L (1996) A study of paleo-magnetic and structure evolution. In: *Advance on Petroleum Geology in Tarim Basin* (eds Tong X, Liang D, Jia C), pp. 196–205. Publishing House of Sciences, Beijing.

Fisher JB, Boles JR (1990) Water-rock interaction in Tertiary sandstones, San Joaquin Basin, California, USA – diagenetic controls on water compositions. *Chemical Geology*, **82**, 83–101.

Ford DC, Ewers RO (1978) The development of limestone cave systems in the dimensions of length and depth. *Canadian Journal of Earth Sciences*, **15**, 1783–98.

Goldstein RH (1986) Reequibriation of fluid inclusions in low-temperature calcium-carbonate cement. *Geology*, **14**, 792–5.

Goldstein RH, Reynolds TJ, 1994. Systematics of fluid inclusions in diagenetic minerals: Society for Sedimentary Geology (SEPM) Short Course 31, 199.

Halley RB, Schmoker JW (1983) High porosity Cenozoic carbonate rocks of south Florida: progressive loss of porosity with depth. *AAPG Bulletin*, **67**, 191–200.

Hu SB, Zhang RY (1998) Methods of thermal history reconstruction in oil-gas basin. *Petroleum Exploration*, **3**, 56–61.

Jia CS, Ma XJ, Rao D, Gao RX (2007) Isotopic characteristics of oil filed waters from Ordovician oil accumulations in Tahe Oilfield and its geological significances. *Acta Sedimentologica Sinica*, **29**, 292–7.

Jiang MS, Zhu JQ, Chen DZ, Zhang RH, Qiao GS (2001) Carbon and strontium isotope variations and responses to sea-level fluctuations in the Ordovician of the Tarim Basin. *Science in China Series D – Earth Sciences*, **44**, 816–23.

Jing JE, Wei WB, Mei ZW (2005) Discussion on development regularities of Karst cave on top of the Ordovician of Tahe Oilfield and relation in oil-gas. *Journal of Jilin University (Earth Science Edition)*, **35**, 622–5.

Lohmann KC (1988) Geochemical patterns of meteoric diagenetic systems and their application to syudies of paleokarst. In: *Paleokarst* (eds James NP, Choquette PW), pp. 58–80. Springer-Verlag, New York.

Louks RG (1999) Paleocave carbonate reservoirs: origins, burial-depth modifications, spatial complexity, and reservoir implications. *American Association of Petroleum Geologists*, **83**, 1795.

Lucia FL (1995) Lower Paleozoic cavern development, collapse, and dolomitization, Franklin Mountains, El Paso, Texas. In: *Unconformities and porosity in carbonate strata. AAPG Memoir* (eds Budd DA, Saller AH, Harris PM), pp. 279–300. AAPG, Tulsa, OK.

Machel HG, Lonnee J (2002) Hydrothermal dolomite – a product of poor definition and imagination. *Sedimentary Geology*, **152**, 163–71.

McLimans RK (1987) The application of fluid inclusions to migration of oil and diagenesis in petroleum reservoirs. *Applied Geochemistry*, **2**, 585–603.

Moore CH, 2001. *Carbonate reservoirs: porosity evolution and diagenesis in a sequence stratigraphic framework*. Elsevier, Amsterdam, London, p. 444.

Muchez P, Nielsen P, Sintubin M, Lagrou D (1998) Conditions of meteoric calcite formation along a Variscan fault and their possible relation to climatic evolution during the Jurassic-Cretaceous. *Sedimentology*, **45**, 845–54.

O'Neil JR, Clayton RN, Mayeda TK (1969) Oxygen isotope fractionation in divalent metal carbonates. *Journal of Chemical Physics*, **51**, 5547.

Prezbindowski DR, Larese RE (1987) Experimental stretching of fluid inclusions in calcite – Implications for diagenetic studies. *Geology*, **15**, 333–6.

Qian YX, Conxita T, Zou SL, You DH, Wang RY (2007) Diagenesis Comparison between Epigenic Karstification and Burial Dissolution in Carbonate Reservoirs: an instance of Ordovician Carbonate Reservoirs in Tabei and Tazhong Regions, Tarim Bain. *Marine Origin Petroleum Geology*, **12**(2), 1–7.

Qian YX, Chen QL, Chen Y, Luo YM (2009) Mineralogical and geochemical identification for diagenetic settings of Paleo-caves and fractures-filling & vugs calcites in carbonate: taking wells S79 and S85 for example. *Acta Sedimentologica Sinica*, **27**, 1027–32.

Qing HR, Mountjoy E (1992) Large-scale fluid-flow in the Middle Devonian Presquile Baresquile Barrier, western Canada Sedimentary Basin. *Geology*, **20**, 903–6.

Qing HR, Mountjoy EW (1994) Origin of dissolurion vugs, caverns, and breccisa in the middle Devonian Presquile barrier, host of Pine Point Mississippi Valley-type deposits. *Economic Geology*, **89**, 858–76.

Sandstrom B, Tullborg EL (2009) Episodic fluid migration in the Fennoscandian Shield recorded by stable isotopes, rare earth elements and fluid inclusions in fracture minerals at Forsmark, Sweden. *Chemical Geology*, **266**, 135–51.

Schwinn G, Wagner T, Baatartsogt B, Markl G (2006) Quantification of mixing processes in ore-forming hydrothermal systems by combinaiton of stable isotope and fluid inclusion analyses. *Geochemica et Cosmochimica Acta*, **70**, 965–82.

Shelton KL, Bauer RM, Gress JM (1992) Fluid-inclusion studies of regionally extensive epigenetic dolomites, Bonneterre Dolomite (Cambrian), southeast Missouri: evidence of multiple fluids during dolomitization and lead-zinc mineralization. *Geological Society of America Bulletin*, **104**, 675–83.

Worden RH, Matray JM (1995) Cross formational flow in the Paris Basin. *Basin Research*, **7**, 53–66.

Worden RH, Warren EA, Smalley PC, Primmer TJ, Oxtoby NH (1995) Evidence for resetting of fluid inclusion termperatures from quartz cements in oilfields – discussion. *Marine and Petroleum Geology*, **12**, 566–70.

Worden RH, Smalley PC, Oxtoby NH (1996) The effects of thermochemical sulfate reduction upon formation water salinity and oxygen isotopes in carbonate gas reservoirs. *Geochimica et Cosmochimica Acta*, **60**, 3925–31.

Worden RH, Manning DAC, Bottrell SH (2006) Multiple generations of high salinity formation water in the Triassic Sherwood Sandstone reservoir: Wytch Farm oilfield, onshore UK. *Applied Geochemistry*, **21**, 455–75.

Yan XB (2002) Paleokarst and reservoir characteristics of Lower Ordovician in Tahe Oilfield. *Journal of Jianghan Petroleum Institute*, **24**, 23–5.

Yu RL (2005) Characteristics and significance of the Caledonian karst in the Tahe oil field, the Tarim basin. *Petroleum Geology & Experiment*, **27**, 468–78.

Zhang K, Wang DR (2004) Types of karst-fractured and porous reservoirs in China's carbonates and the nature of the Tahe Oilfield in the Tarim Basin. *Acta Geologica Sinica – English Edition*, **78**, 866–72.

Zhang DJ, Lv HT, Zhang T, Wu XW (2007) Characteristics of Caledonian Karstification Reservoir in Tahe Oilfield and Its Distribution. *Acta Sedimentologica Sinica*, **25**, 214–23.